Coherent-states dynamics of the H++C2H2 reaction at ELab=30eV: A complete electron nuclear dynamics investigation

ARTICLE *in* CHEMICAL PHYSICS LETTERS · OCTOBER 2005

Impact Factor: 1.9 · DOI: 10.1016/j.cplett.2005.08.086

7 AUTHORS, INCLUDING:

Yunan Yan
Guizhou Normal College, Guiyang, China
27 PUBLICATIONS **262** CITATIONS
SEE PROFILE

Kakha Tsereteli
BSE networks
6 PUBLICATIONS **115** CITATIONS
SEE PROFILE

Christopher G. Myers
University of Texas Medical Branch at Galve…
3 PUBLICATIONS **19** CITATIONS
SEE PROFILE

Available online at www.sciencedirect.com
SCIENCE DIRECT®
Chemical Physics Letters 414 (2005) 405–411
CHEMICAL PHYSICS LETTERS
www.elsevier.com/locate/cplett

Coherent-states dynamics of the $H^+ + C_2H_2$ reaction at $E_{Lab} = 30$ eV: A complete electron nuclear dynamics investigation

Jorge A. Morales *, Buddhadev Maiti, Yunan Yan, Kakha Tsereteli, Jennifer Laraque, Srirangam Addepalli, Chris Myers

Department of Chemistry and Biochemistry, Texas Tech University, P.O. Box 41061, Lubbock, TX 79409-1061, USA

Received 21 June 2005; in final form 3 August 2005
Available online 13 September 2005

Abstract

Preliminary results of an exhaustive study of $H^+ + HC{\equiv}CH$ at $E_{Lab} = 30$ eV within the electron nuclear dynamics (END) and coherent state dynamics (CSD) theories are herein presented. Current END–CSD method employs frozen Gaussian wave packets in the semiclassical limit of $\hbar \to 0$ for the nuclei and a single-determinantal Thouless coherent state (CS) for the electrons. The simulated 6800 trajectories from 68 independent $HC{\equiv}CH$ target orientations provide a definite description of all the reactive processes, including H_2 formation and charge transfers. Differential and integral cross-sections are evaluated via a novel CS S-matrix formulation in conjunction with semiclassical techniques. Calculated cross-sections show a good agreement with both experimental and previous END results.

1. Introduction

During the last decades, research on proton–molecule collisions has enjoyed an upsurge of interest as a technique to study flames, materials, plasmas, upper atmosphere reactions, and astrophysical phenomena [1–8]. Proton light mass favors short collision times, simplifies the kinematical interpretation of post-collision angular distributions, and enhances energy loss resolution. More importantly, a structureless proton cannot undergo itself inelastic rovibrational transitions but does provoke and localize those processes on its collisional counterpart. Moreover, a proton can accept one electron from a molecular target and consequently probe charge-transfer reactions (CTR).

Several experimental studies of proton–molecule collisions exist in the literature [1] and those by the Toennies group [2–8] are the most detailed and systematic. This group has extensively measured several proton–molecule reactions at projectile collisional energies of about $10 \leqslant E_{Lab} \leqslant 46$ eV and performed time-of-flight vibrational analyses of non-charge-transfer (protons) and charge-transfer (hydrogen atoms) outgoing projectiles scattered from several target molecules, including: H_2 [2], O_2 [3], H_2O [4], CO_2 [5], N_2O [5], C_2H_2 [6], CH_4 [7], CF_4 [8], and SF_6 [8] inter alia.

Toennies group studies have set the stage for fruitful interactions between experimental and theoretical techniques because its measurements can be used to assess the accuracy of a theoretical method whereas the latter can elucidate reaction details unattainable experimentally. However, due to the complexity of the investigated systems, few of them have been examined theoretically with advanced quantum methodologies, being a worthy exception the simulation of the $H^+ + H_2$ collision [2], first with the trajectory surface hopping method (TSHM) [2,9] and finally with the higher-level infinite order sudden approximation (IOSA) [10]. This situation finally changed when Morales et al. applied systematically the electron nuclear dynamics (END) theory [11] to the reactions: $H^+ + H_2$ [12,13], $H^+ + CH_4$ [14], and $H^+ + H_2O$ [15], and obtained excellent agreements with the Toennies group results. One of the reasons for such a success stems from the END intrinsic flexibility to take into account all the possible reactive processes involved.

* Corresponding author. Fax: +1 806 742 1289.
E-mail address: jorge.morales@ttu.edu (J.A. Morales).

0009-2614/$ - see front matter © 2005 Elsevier B.V. All rights reserved.
doi:10.1016/j.cplett.2005.08.086

One of the most interesting experiments by the Toennies group was that on the proton–acetylene collision, $H^+ + CH{\equiv}CH$, at $E_{Lab} = 30$ eV [6], because it quantitatively probed several chemical processes (vibrational excitation, energy and electron transfers) in a system of organic chemistry relevance. Malinovskaya et al. [16] undertook the first END study of the $H^+ + CH{\equiv}CH$ system and obtained an excellent agreement with the experimental results. However, their inspiring END simulations only considered three orientations of the CH≡CH target molecule, which cannot fully account for the rich chemistry of this system. Therefore, we present herein the preliminary results of an exhaustive END study of the $H^+ + CH{\equiv}CH$ system that considers all the relevant target orientations to describe its complex reactivity and to consummate the pioneering efforts in [16].

2. Theoretical background

The END theory was created by Deumens and Öhrn [11]. Herein, we will briefly outline END in the context of our novel and unifying coherent-states dynamics (CSD) theory that supplies coherent states (CS) for all the molecular degrees of freedom: translational, rotational, vibrational and electronic. Even with the present computer technology, full quantum mechanical descriptions of large systems remain unfeasible and recurrences to less costly classical mechanics treatments are inescapable for some degrees of freedom. A practical methodology to treat large systems should be one that allows transitions from quantum to classical mechanics in a gradual and continuous way, and at any desired level of accuracy. Such flexibility can be obtained by exploiting the properties of CS [17]. Broadly speaking, CS are sets of genuine quantum states that permit expressing full quantum dynamical equations in a classical-like Hamiltonian format (symplectic structure [18,19]) in terms of generalized positions and conjugate momenta: q_i and p_i. More formally, the states $|z_i\rangle$, depending upon the complex parameters $z_i = q_i + ip_i$, make a set of CS if they satisfy the following two conditions [17]: (I) continuity with respect to z_i; and (II) resolution of unity: $1 = \int d\mu(z_i)|z_i\rangle\langle z_i|$ with positive measure $d\mu(z_i) > 0$ and $\langle z_i \mid z_i'\rangle \neq 0$ (i.e. a non-orthogonal, over-complete basis set [17]). Some CS are also quasi-classical [20] in the sense that there exists a Hamiltonian $\hat{H}$ so that the CS average position and momenta are $\langle \hat{x}_i\rangle = q_i(t) = \langle z_i(t)|\hat{x}_i|z_i(t)\rangle$ and $\langle \hat{p}_i\rangle = p_i(t) = \langle z_i(t)|\hat{p}_i|z_i(t)\rangle$, and evolve in time with $\hat{H}$ according to Hamilton classical equations: $\dot{q}_i = \partial H(q_i, p_i)/\partial p_i$ and $\dot{p}_i = -\partial H(q_i, p_i)/\partial q_i$, with $H(q_i, p_i) = \langle z_i(t)|\hat{H}|z_i(t)\rangle$. A CS-parameterized dynamics is still quantum mechanical but in the closest possible form to classical mechanics; if the CS is also quasi-classical then a classical dynamics with a quantum state is obtained. Most of the CS herein described are constructed via the Lie group Perelomov Prescription (PP), whose intricate details are explained in [17]. However, PP does not automatically generate a quasi-classical CS. Non-trivial departures from PP to enforce quasi-classical behavior and exceptions to the two CS conditions are discussed in [20].

For a molecular system with N_{Nucl} nuclei and N_{el} electrons, the simplest END–CSD total wavefunction ψ_{Total} is the product of nuclear ψ_{Nucl} and electronic ψ_{el} parts: $\psi_{Total} = \psi_{Nucl}\psi_{el}$. ψ_{Nucl} is a product of $3N_{Nucl}$ narrow-width, frozen Gaussian wave packets:

$$\psi_{Nucl}(\mathbf{X};\mathbf{R},\mathbf{P}) = \prod_{i=1}^{3N_{Nucl}} \exp\left\{-\left(\frac{X_i - R_i}{2\Delta R_i}\right)^2 + \frac{iP_i}{\hbar}(X_i - R_i)\right\}, \tag{1}$$

with average positions R_i, average momenta P_i, and position normal deviation $\Delta R_i \propto \hbar^{1/2}$. ψ_{Nucl} is also factorized into translational, rotational and vibrational parts: $\psi_{Nucl} = \psi_{Trans}\psi_{Rot}\psi_{Vib}$. ψ_{Trans} is a CS wave packet describing quasi-classically the center of mass (CM) motion [20,21]. ψ_{Rot} is approximately the nearly quasi-classical Morales rotational CS $\psi_{Rot} = |\alpha\beta\gamma\rangle$ [20,21] via a departure from the PP treatment of the $SO(3) \otimes SO(3) \otimes A$ Lie group. ψ_{Vib} is a product of $3N_{Nucl}$–6 quasi-classical Glauber CS [13] $\psi_{Vib} = \prod_{i=1}^{3N_{Nucl}-6}|z_i\rangle$. For ψ_{el}, K fermion creation (annihilation) operators $b_i^\dagger$ (b_i) of N_{el} occupied $\{\phi_h\}$ and $K-N_{el}$ virtual $\{\phi_p\}$ orthogonal molecular spin–orbitals (MSO) can generate particle–hole pairs operators $b_p^\dagger b_h$ of the $U(K)$ Lie group [17]. Taking as a fiducial state the Fermi vacuum single determinant $|0\rangle = b_{N_{el}}^\dagger \ldots b_1^\dagger|\text{vac}\rangle$, the non-quasi-classical, single-determinantal Thouless electronic CS $|\boldsymbol{\mu};\mathbf{R}\rangle$ [17,22,23], in terms of the non-orthogonal Thouless MSO $\{\chi_h\}$, $\chi_h = \phi_h + \sum_{p=N_{el}+1}^{K}\phi_p\mu_{ph}(1 \leqslant h \leqslant N_{el})$ [22,23], is

$$\begin{aligned}\psi_{el} = |\boldsymbol{\mu};\mathbf{R}\rangle &= \det[\chi_h(\boldsymbol{\mu};\mathbf{R})] \\ &= \exp\left(\sum_{p=N_{el}+1}^{K}\sum_{h=1}^{N_{el}}\mu_{ph}(t)b_p^\dagger b_h\right)|0\rangle \\ &= |0\rangle + \sum_{p,h}\mu_{ph}(t)b_p^\dagger b_h|0\rangle \\ &\quad + \sum_{p,h,p',h'}\mu_{ph}(t)\mu_{p'h'}(t)b_p^\dagger b_{p'}^\dagger b_{h'}b_h|0\rangle + \cdots \text{etc.},\end{aligned} \tag{2}$$

where $b_p^\dagger b_h|0\rangle$, $b_p^\dagger b_{p'}^\dagger b_{h'}b_h|0\rangle$, etc., are singly, doubly excited, etc., single determinants out of $|0\rangle$. The orthogonal MSO $\{\phi_h, \phi_p\}$ are formed from Gaussians centered on the nuclear wave packets and depend upon $\{R_i\}$ and so does $|\boldsymbol{\mu};\mathbf{R}\rangle$. Those MSO are unrestricted so that $|\boldsymbol{\mu};\mathbf{R}\rangle$ can describe both closed-shell $H^+ + HC{\equiv}CH$ and open-shell $H^0 + HC{\equiv}CH^+$ separations [24,25]. Thouless CS provides a non-redundant representation of a general single-determinantal state $|\boldsymbol{\mu};\mathbf{R}\rangle$ out of and non-orthogonal to $|0\rangle$ [22,23]. $|\boldsymbol{\mu};\mathbf{R}\rangle$ is at the same time one single determinant in terms of the non-orthogonal Thouless MSO $\{\chi_h\}$ and also a superposition of the excited single determinants out of $|0\rangle$ in terms of the orthogonal MSO $\{\phi_h, \phi_p\}$. Those excited single determinants represent different non-charge-transfer and charge-transfer channels. A multi-configuration electronic CS [26] would be more adequate to describe

the multi-channel $H^+ + HC{\equiv}CH$ reaction but has not been implemented yet. Nevertheless, the present single-determinantal Thouless CS comprising singly and higher-excited single determinants renders satisfactory results as shown below.

With ψ_{Total} CS-formulated, the quantum Lagrangian is $\mathscr{L}_{\text{CS}} = \langle\psi_{\text{Total}}|[\frac{i\hbar}{2}(\frac{\vec{\partial}}{\partial t} - \frac{\vec{\partial}}{\partial t}) - \hat{H}|\psi_{\text{Total}}\rangle/\langle\psi_{\text{Total}}|\psi_{\text{Total}}\rangle$ [19]. By imposing stationarity to the quantum action A_{CS}, $\delta A_{\text{CS}} = \delta\int_{t_1}^{t_2}\mathscr{L}_{\text{CS}}(t)\mathrm{d}t = 0$ [11,19] with the nuclei in the semiclassical limit of $\hbar \to 0$, the END dynamical equations for the CS parameters R_i, P_i, μ_{ph}, and μ^*_{ph} are obtained [11,19]:

$$\begin{bmatrix} \mathbf{iC} & \mathbf{0} & \mathbf{iC_R} & \mathbf{0} \\ \mathbf{0} & -\mathbf{iC}^* & -\mathbf{iC}^*_{\mathbf{R}} & \mathbf{0} \\ \mathbf{iC}^\dagger_{\mathbf{R}} & -\mathbf{iC}^{\mathrm{T}}_{\mathbf{R}} & \mathbf{C_{RR}} & -\mathbf{I} \\ \mathbf{0} & \mathbf{0} & \mathbf{I} & \mathbf{0} \end{bmatrix} \begin{bmatrix} \frac{\mathrm{d}\boldsymbol{\mu}}{\mathrm{d}t} \\ \frac{\mathrm{d}\boldsymbol{\mu}^*}{\mathrm{d}t} \\ \frac{\mathrm{d}\mathbf{R}}{\mathrm{d}t} \\ \frac{\mathrm{d}\mathbf{P}}{\mathrm{d}t} \end{bmatrix} = \begin{bmatrix} \frac{\partial E_{\text{Total}}}{\partial \boldsymbol{\mu}^*} \\ \frac{\partial E_{\text{Total}}}{\partial \boldsymbol{\mu}} \\ \frac{\partial E_{\text{Total}}}{\partial \mathbf{R}} \\ \frac{\partial E_{\text{Total}}}{\partial \mathbf{P}} \end{bmatrix}, \tag{3}$$

where the left matrix is the inverse of Hamilton generalized symplectic matrix [18,19] with dynamical sub-matrices containing non-adiabatic coupling terms:

$$(\mathbf{C}_{XY})_{ij:kl} = -2\mathrm{Im}\frac{\partial^2 \ln S}{\partial X_{ik}\partial Y_{jl}}\bigg|_{\mathbf{R}'=\mathbf{R}};$$
$$(\mathbf{C}_{X_{ik}})_{\text{ph}} = \frac{\partial^2 \ln S}{\partial \mu^*_{\text{ph}}\partial X_{ik}}\bigg|_{\mathrm{R}'=\mathbf{R}}; \quad \mathbf{C}_{\text{ph:qg}} = \frac{\partial^2 \ln S}{\partial \mu^*_{\text{ph}}\partial \mu_{\text{qg}}}\bigg|_{\mathbf{R}'=\mathbf{R}}, \tag{4}$$

where $S = \langle\boldsymbol{\mu}';\mathbf{R}'|\boldsymbol{\mu};\ \mathbf{R}\rangle$ is the overlap between two Thouless CS and $E_{\text{total}} = \langle\psi_{\text{Total}}|\hat{H}|\psi_{\text{Total}}\rangle/\langle\psi_{\text{Total}}|\psi_{\text{Total}}\rangle = \sum_{i=1}^{3N_{\text{Nucl}}}P_i^2/2M_i + \langle\boldsymbol{\mu};\ \mathbf{R}|\widehat{H}_{\text{el}}|\boldsymbol{\mu};\mathbf{R}\rangle/\langle\boldsymbol{\mu};\mathbf{R}|\boldsymbol{\mu};\mathbf{R}\rangle$ the total energy. Eq. (3) expresses in a quantum Hamilton symplectic format [19] the combined quantum electronic and quasi-classical CM, rotational and vibrational CS dynamics. Eq. (3) treats simultaneously both electron and nuclei and provides a direct dynamics not requiring pre-calculated potential energy surfaces to run. The CS parameters R_i, P_i, μ_{ph}, and μ^*_{ph} evolving in time trace different reaction trajectories in a CS quantum phase space. In a simulation, reactants are prepared with initial positions and momenta: R_i^0, and P_i^0, and with electronic state μ^0_{ph}, and μ^{0*}_{ph} (Fig. 1) to define the initial wave function $\psi^{\text{i}}_{\text{Total}} = \psi^0_{\text{Total}}$. A chemical reaction simulation is advanced by integrating Eq. (3) over time. Initially, all μ_{ph} can be zero, $\mu_{\text{ph}} = 0 \Rightarrow |\boldsymbol{\mu};\ \mathbf{R}\rangle = |0\rangle, |0\rangle$ being an unrestricted Hartree–Fock (UHF) self-consistent field (SCF) single determinant [24,25] describing an incoming asymptotic $H^+ + HC{\equiv}CH$. Eventually, the CS parameters $\mu_{\text{ph}}(t)$ will assume non-zero values and the excited single determinants of Eq. (2) will appear. Some of the singly excited single determinants will correspond to non-charge-transfer outgoing channels $H^+ + HC{\equiv}CH$ and others to charge-transfer ones $H^0 + HC{\equiv}CH^+$ depending upon the MSO $\{\phi_{\text{h}}, \phi_{\text{p}}\}$ implicated in the excitations. At the final time, the evolved wavefunction $\psi^{\infty}_{\text{Total}}$ can be projected onto selected reaction products eigenstates $\psi^{\text{f}}_{\text{Total}} = \psi^{\text{f}}_{\text{Trans}}\psi^{\text{f}}_{\text{Rot}}\psi^{\text{f}}_{\text{Vib}}\psi^{\text{f}}_{\text{el}}$ so that the quantum probability amplitude $S^{\text{i}\to\text{f}}_{\text{CS}}$ for the transition $\psi^{\text{i}}_{\text{Total}} \to \psi^{\text{f}}_{\text{Total}}$ is

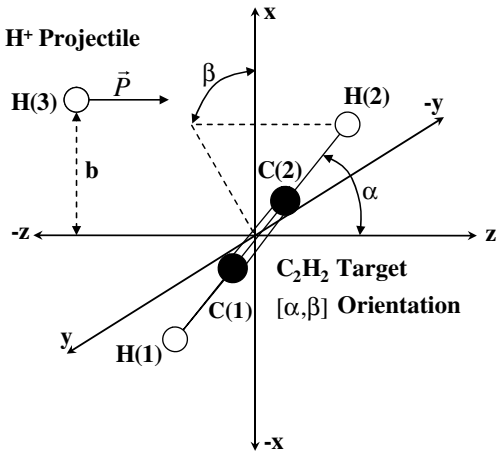

Fig. 1. $H^+ + HC{\equiv}CH$ reactants initial conditions; balls represent nuclear wave packets for the atoms with projectile impact parameter b and target orientation $[\alpha, \beta]$.

$$S^{\text{i}\to\text{f}}_{\text{CS}} = \langle\psi^{\text{f}}_{\text{Total}}|\psi^{\infty}_{\text{Total}}\rangle = A^{\text{i}\to\text{f}}_{\text{Trans}}A^{\text{i}\to\text{f}}_{\text{Rot}}A^{\text{i}\to\text{f}}_{\text{Vib}}A^{\text{i}\to\text{f}}_{\text{el}}\exp\left(\frac{\mathrm{i}A_{\text{CS}}}{\hbar}\right), \tag{5}$$

where each $A^{\text{i}\to\text{f}}_{\text{Degree}}$ is a reaction transition probability amplitude per degree (e.g. $A^{\text{i}\to\text{f}}_{\text{Trans}} = \langle\psi^{\text{f}}_{\text{Trans}}|\psi^{\infty}_{\text{Trans}}\rangle$). All relevant properties of a chemical reaction (e.g. differential and integral cross-sections, rate constants) can be calculated from the probability amplitude $S^{\text{i}\to\text{f}}_{\text{CS}}$.

3. Computational details

All calculations have been performed with the program CSTechG, developed from the ENDyne 2.7 and 2.8 codes (E. Deumens, ENDyne: Electron Nuclear Dynamics Simulations, Version 2 Release 8, Quantum Theory Project: University of Florida, Gainesville, FL 32611-8435, 1997) and containing new CS and electronic-structure capabilities along with compute grid implementations for Microsoft Windows® and Red Hat Linux® operating systems inter alia. The nuclear CS parameters defining the reactants initial conditions are shown in Fig. 1. The nuclei originally in the $CH{\equiv}CH$ molecule are labeled C(1), C(2), H(1) and H(2), respectively, and the incoming H^+ projectile H(3). To expedite these costly simulations, the STO-3G basis set [25] is herein used for the MSO instead of the pVDZ one of [16]. Previous END/STO-3G studies of the $H^+ + CH_4$ reaction [14] have firmly demonstrated the STO-3G sufficiency to describe the main features of proton–molecule reactions. Furthermore, a few $H^+ + CH{\equiv}CH$ tests with the pVDZ basis sets did not show significant differences with the present results. The $CH{\equiv}CH$ target molecule is initially at rest ($P_{\text{i}} = 0$) and in its electronic ground state at the UHF-SCF/STO-3G level [24,25]. The angular orientation $[\alpha, \beta]$ of the target molecule is determined by the polar and azimuthal angles: $0° \leqslant \alpha \leqslant 180°$ and $0° \leqslant \beta \leqslant 360°$, respectively. The H^+ projectile is initially placed at (b, 0.0, –15.00 a.u.) where b is the impact parameter. The projectile initially travels in the

positive z-direction with P_z^{in} corresponding to $E_{\text{Lab}} = 30$ eV. Two distinct sets of trajectories are calculated from varying initial conditions. Set 1 comprises target initial orientations $[\alpha, \beta]$ with $0° \leqslant \alpha \leqslant 180°$ in steps $\Delta\alpha = 11.25°$ and with $\beta = 0°$, 45° and 90°, and with projectile initial impact parameters: $0.0 \leqslant b \leqslant 9.9$ a.u. in steps $\Delta b = 0.1$ a.u. without duplicating symmetry equivalent trajectories (e.g. $[\alpha, 90°] \equiv [180° - \alpha, 90°]$); Set 2 comprises 'orthogonal' collisions with the target at initial orientations $[90°, \beta]$ with β in two ranges: $0° \leqslant \beta \leqslant 16°$ in steps $\Delta\beta = 1°$ and $20° \leqslant \beta \leqslant 90°$ in steps $\Delta\beta = 5°$, respectively, and with b as in Set 1. This produces a total of 68 independent target orientations and 6800 different trajectories, making the present END–CSD study be the most exhaustive hitherto undertaken. END–CSD/STO-3G calculations are run for 1000 a.u. of time from the initial conditions, with a few longer simulations of up to 5000 a.u. in the most complex cases. After the simulations are complete, several programs in the CSTechG suite analyze the well-separated products and calculate dynamical properties.

4. Results and discussion

4.1. Reactivity

The present system displays an astonishing variety of reactive processes. Theoretically predicted product channels include: (a) non-transfer scattering (NTS)

$$\text{H}^+ + \text{H–C}{\equiv}\text{C–H}\ (v_\text{i}, l_\text{i}) \rightarrow \text{H}^+ + \text{H–C}{\equiv}\text{C–H}\ (v_\text{f}, l_\text{f})\ \text{(NTS)}, \tag{6}$$

(b) charge-transfer scattering (CTS)

$$\text{H}^+ + \text{H–C}{\equiv}\text{C–H}\ (v_\text{i}, l_\text{i}) \rightarrow \text{H}^0 + \text{H–C}{\equiv}\text{C–H}^{\oplus}\ (v_\text{f}, l_\text{f})\ \text{(CTS)}, \tag{7}$$

NTS and CTS happen together with probability amplitudes $\propto A_{\text{el}}^{\text{i}\rightarrow\text{f}}$; (c) collision-induced carbon-hydrogen dissociation (C–H D)

$$\begin{aligned}&\text{H}^+ + \text{H–C}{\equiv}\text{C–H}\ (v_\text{i}, l_\text{i})\\ &\quad\rightarrow \text{H}^q + \text{H}^{q'} + \text{C}{\equiv}\text{C–H}^{q''}(v_\text{f}, l_\text{f})\ \text{(C–H D)}\\ &\quad q + q' + q'' = +1,\end{aligned} \tag{8}$$

sometimes associated with a C–H strong vibration (C–H SV); (d) collision-induced carbon–carbon dissociation (C≡C D)

$$\begin{aligned}&\text{H}^+ + \text{H–C}{\equiv}\text{C–H}\ (v_\text{i}, l_\text{i})\\ &\quad\rightarrow \text{H}^q + \text{C–H}^{q'} + \text{C–H}^{q''}(v_\text{f}, l_\text{f})\ \text{(C}{\equiv}\text{C D)}\\ &\quad q + q' + q'' = +1,\end{aligned} \tag{9}$$

(e) hydrogen rearrangement (HR)

$$\begin{aligned}&\text{H}^{+\bullet} + \text{H–C}{\equiv}\text{C–H}\ (v_\text{i}, l_\text{i})\\ &\quad\rightarrow \text{H}^q + \text{H–C}{\equiv}\text{C–H}^{q'\bullet}(v_\text{f}, l_\text{f})\ \text{(HR)}\\ &\quad q + q' = +1,\end{aligned} \tag{10}$$

where $\bullet$ labels the exchanged hydrogen atom; and finally (f) H_2 formation (H_2-F)

$$\text{H}^+ + \text{H–C}{\equiv}\text{C–H}\ (v_\text{i}, l_\text{i}) \rightarrow \text{H}_2 + \text{C}{\equiv}\text{C–H}^{\oplus}(v_\text{f}, l_\text{f})\ \text{(H}_2\text{-F)}. \tag{11}$$

No H_2^+ formation is predicted. Above, $(v_\text{i}, l_\text{i}) \rightarrow (v_\text{f}, l_\text{f})$ labels the initial and final vibrational and rotational states, respectively, since all the channels exhibit rovibrational inelasticity. Processes (c) to (e) also contribute to charge-transfer reactions (CTR) via the outgoing projectile H^q with finite probability of having $q = 0$. Trajectories from orientations $[\alpha, 45°]$ and $[\alpha, 90°]$ only exhibit NTS/CTS whereas the remaining ones display the full gamut of the above reactions. Reactions for selected $[\alpha, 0°]$ orientations vs. b are listed in Table 1 whereas those for the $[90°, \beta]$ orientations are depicted in Fig. 2. Generally, C–H D, C≡C D, HR and H_2-F happen for small b whereas NTS/CTS for large ones. One H_2-F is illustrated in Fig. 3 for $[112.5°, 0°]$ and $b = 2.3$ a.u. by plotting the atoms positions on the x–z plane. H_2-F only happens in the $[\alpha > 90°, 0°]$ orientations and was not therefore detected in the three orientations: [0°, 0°], [90°, 0°] and [90°, 90°] of [16].

4.2. Scattering angles and rainbow angles

The outgoing H^q ($q = +1,0$) projectile scattering angle θ with respect to the incoming z-direction is determined by

$$\sin\theta = \frac{(P_x^{\text{out}\,2} + P_y^{\text{out}\,2})^{1/2}}{(P_x^{\text{out}\,2} + P_y^{\text{out}\,2} + P_z^{\text{out}\,2})^{1/2}}; \quad 0 \leqslant \theta \leqslant 180°, \tag{12}$$

where the P_i^{out} are the outgoing projectile momentum components at final time. Fig. 4 displays $\theta(b)$ vs. b for some representative orientations. All simulations exhibit a primary rainbow peak ($[\frac{\text{d}\theta(b)}{\text{d}b}]_{b=b_{\text{pr}}} = 0$, maximum) at high b. At lower b, $[\alpha, 90°]$ and $[90°, 90°]$ orientations exhibit one glory angle $\theta_{\text{Glory}}(b_{\text{Glory}}) = 0$ that in the remaining orientations degenerates into a secondary rainbow peak ($[\frac{\text{d}\theta(b)}{\text{d}b}]_{b=b_{\text{sr}}} = 0$, minimum) associated with the projectile scattering off the original x–z plane. Secondary rainbow angles were also observed in the $H^+ + H_2$ system [13] inter alia. Primary and secondary rainbow angles for some selected orientations are listed in Table 2. Fig. 4 shows the typical pattern of transitions from repulsive to attractive scattering when going from low to high b's, neither-repulsive-nor-attractive interactions at b_{Glory}, and primary rainbow angles where attractive interactions reach their maximum. Unlike $H^+ + H_2$ [12,13], the calculated rainbow angles distribute uniformly over all the target orientation $[\alpha, \beta]$ (e.g. the primary rainbow angle varies: 3.7°[90°, 10°]–14.9°[168.75°, 0°] and lie well in their experimentally inferred range of 1°–12° [6].

4.3. Total differential cross-section

The main result of the Toennies group experiment is the total NTS/CTS differential cross-section (DCS). The

Table 1
Reactive processes for some [α, 0°] orientation vs. impact parameter b

Orientation [α, β] (°)	Impact parameter, b (a.u.)	Reactive process
[0, 0]	0.0	NTS/CTS
	0.1	C–H D or HR
	0.2–0.5	C–H D
	0.6–9.9	NTS/CTS
[22.5, 0]	0.0–1.4	NTS/CTS
	1.5–3.4	C–H D
	3.5–9.9	NTS/CTS
[45, 0]	0.0–1.8	NTS/CTS
	1.9–2.0	NTS/CTS/C–H D
	2.1–3.2	C–H D
	3.3–9.9	NTS/CTS
[67.5, 0]	0.0–1.9	NTS/CTS
	2.0–2.4	C–H D
	2.5–3.2	HR
	3.3–4.0	C–H D
	4.1–9.9	NTS/CTS
[90, 0]	0.0–0.1	NTS/CTS
	0.2	C≡C D and C–H D
	0.3	C≡C D
	0.4–1.8	NTS/CTS
	1.9–3.0	C–H D
	3.1–3.4	HR
	3.5–3.7	C–H D
	3.8–9.9	NTS/CTS
[112.5, 0]	0.0–1.5	NTS/CTS
	1.6–1.9	C–H D
	2.0–2.6	H_2-F
	2.7	C–H D
	2.8–3.1	HR
	3.2–3.5	C–H D
	3.6–9.9	NTS/CTS
[135, 0]	0.0–1.2	NTS/CTS
	1.3–2.0	C–H D
	2.1–2.4	HR
	2.5	C–H D
	2.6	H_2-F
	2.7	C–H D
	2.8–9.9	NTS/CTS
[157.5, 0]	0.0–0.7	NTS/CTS
	0.8–1.0	C–H D
	1.1–1.3	HR
	1.4	H_2-F
	1.5–1.8	C–H D
	1.9–9.9	NTS/CTS

NTS, non-transfer scattering; CTS, charge-transfer scattering; C–H D carbon–hydrogen dissociation; C≡C D carbon–carbon dissociation; HR, hydrogen rearrangement; H_2-F, H_2 formation.

inelastic DCS $\left[\frac{d\sigma(\theta)}{d\Omega}\right]_{i\to f}$ from initial to final states $i \to f$ is [27]:

$$\left[\frac{d\sigma(\theta)}{d\Omega}\right]_{i\to f} = \frac{1}{4k_i^2}\left|\sum_{l=0}^{\infty}(2l+1)[S^{i\to f}_{Quantum}(l) - \delta_{if}]P_l(\cos\theta)\right|^2, \quad (13)$$

where k_i is the projectile initial wave vector, l the orbital angular momentum quantum numbers, $S^{i\to f}_{Quantum}(l)$ the S-matrix and $P_l(\cos\theta)$ Legrende polynomials. It is proven

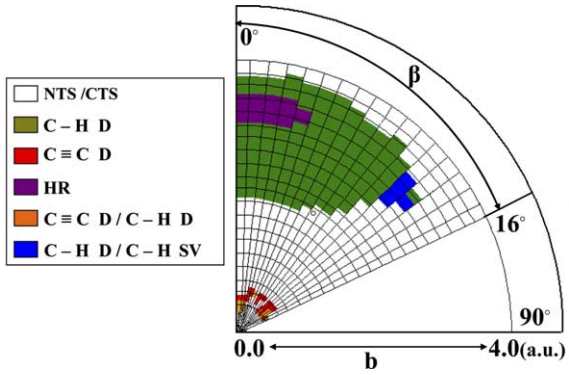

Fig. 2. Reactions for the [90°, β] orientations as a function of the impact parameter (as the radius in a.u.) and of the angle β (degree). The scale for β is not linear to facilitate visualization. Reactions acronyms in text.

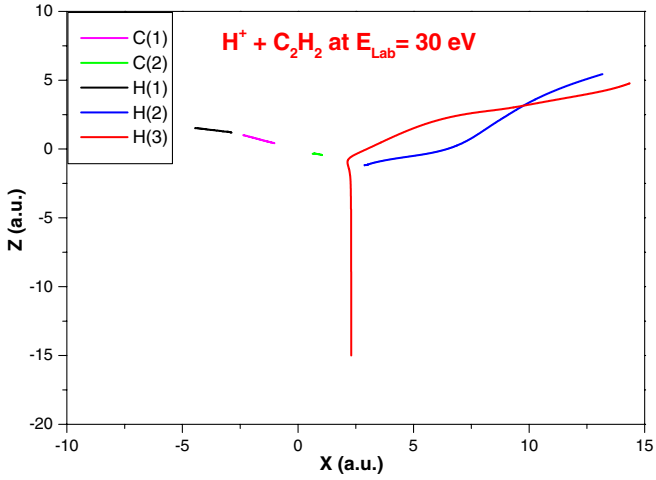

Fig. 3. H_2 formation for [112.5°, 0°] and $b = 2.3$ a.u.; atoms trajectories on the x–z plane.

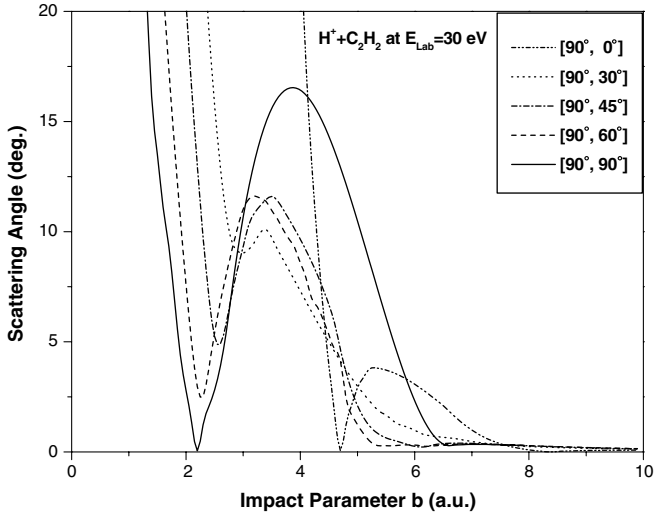

Fig. 4. Scattering angle $\theta(b)$ vs. impact parameter b for selected [α, β] orientations.

Table 2
Primary (quasi-classical and semiclassical) and secondary (quasi-classical) rainbow angles for selected orientations

Orientation [α, β] (°)	Impact parameter, b (a.u.)	Quasi-classical primary rainbow angle, θ_r (°)	Semiclassically corrected primary rainbow angle, θ_r (°)	Quasi-classical secondary rainbow angle, θ_r, (°)
[0, 0]	3.2	13.8	11.1	
[22.5, 0]	3.6	9.5	7.1	
[45, 0]	4.5	6.9	4.5	
[67.5, 0]	5.1	3.4	1.0	
[90, 0]	5.3	3.8	1.3	
[112.5, 0]	5.3	7.4	5.2	
[135, 0]	4.2	12.9	9.8	
[157.5, 0]	3.4	14.9	13.8	
[22.5, 45]	3.5	10.9	8.6	3.3
[45, 45]	3.4	8.1	6.3	5.7
[67.5, 45]	3.5	10.2	8.0	4.8
[90, 45]	3.5	11.6	9.5	4.9

via CS theory [21] that END–CSD DCS can be obtained by evaluating the sum in Eq. (13) in the semiclassical limit of $\hbar \to 0$ and by identifying: $l \sim k_i b$ and $S^{i\to f}_{Quantum} \to S^{i\to f}_{CS}$, Eq. (5), inter alia. For values of b such as $\theta(b)$ is away from rainbow angles, the stationary phase approximation at $\hbar \to 0$ in Eq. (13) renders [21]

$$\left[\frac{d\sigma(\theta)}{d\Omega}\right]_{i\to f} = \left|\sum_{m=1}^{N} \frac{\sqrt{b_m} S^{i\to f}_{CS}(b_m)}{\sqrt{\sin\theta \left[\frac{d\theta(b)}{db}\right]_{b=b_m}}}\right|^2, \qquad (14)$$

where m labels the N trajectories (branches) with impact parameter b_m contributing to the same scattering angle θ. This expression introduces quantum interference through the CS action A_{CS} in $S^{i\to f}_{CS}$ [21], Eq. (5), but produces spurious singularities near primary/secondary rainbow angles where $[\frac{d\theta(b)}{db}]_{b=b_m} = 0$. The uniform Pearcey approximation [28] is the most rigorous semiclassical treatment for DCS exhibiting two close (here primary and secondary) rainbow angles but it is too cumbersome to apply. $H^+ + H_2$ [13], $H^+ + CH_4$ [14] and $H^+ + H_2O$ [15] studies have demonstrated that the simpler uniform Airy approximation [28] suffices in this context. Thus, the quasi-classical rainbow singularity is replaced by the bounded primary maximum of the Airy function [28] thereby rendering semiclassically corrected rainbow angles that for primary rainbows are 1°–3° lower than their quasi-classical originators (Table 2). This makes the END–CSD/STO-3G primary rainbow angles lie even better within the experimental range. The uniform Airy approximation DCS goes uniformly to that of Eq. (14) for θ away from the rainbow angles. Both the END–CSD/STO-3G total NTS/CTS DCS averaged over the 36 [α, β] orientations in Set 1 and the Toennies group result [6] are plotted in Fig. 5. The dispersion of rainbow angles over all the target orientations makes both theoretical and experiential results have a blurred rainbow resolution. Therefore, the un-normalized experimental results are matched to the END–CSD/STO-3G one at the midpoint of the measured θ's ($\theta = 10°$). The agreement between the two results is highly satisfactory despite the limitations of the minimal STO-3G. As with $H^+ + CH_4$ [14], END–CSD/STO-3G seems to predict smaller DCS at low scattering angles, an effect perhaps attributable to a less accurate, long-separation $H^+ - HC{\equiv}CH$ interaction with STO-3G. An ongoing END–CSD basis set study on $H^+ + CH{\equiv}CH$, including STO-3G, pVDZ and 6-31G** basis sets, will scrutinize that conjecture. This study will be presented in a future publication. It is worth noticing that the END–CSD/STO-3G DCS of the orientations [90°, 0°] and [90°, 90°], the most important calculated in [16], agree better with the experiment.

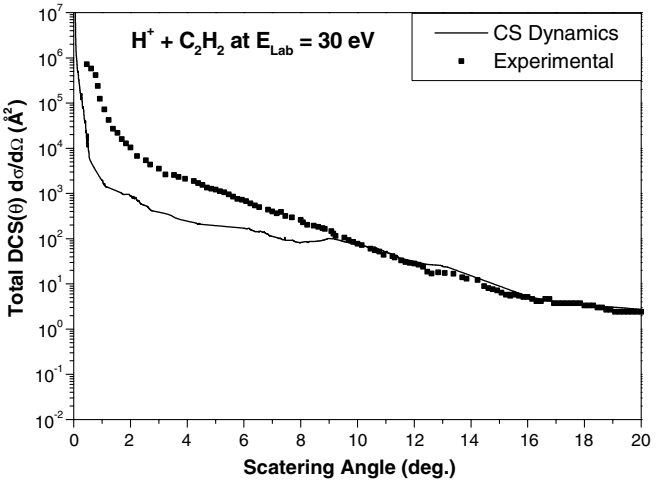

Fig. 5. $H^+ + HC{\equiv}CH$ at $E_{Lab} = 30$ eV END–CSD/STO-3G and experimental ([6]) total differential cross-sections vs. scattering angle θ.

4.4. Charge-transfer reaction integral cross-section

Integral cross-sections (ICS) $\sigma_{i\to f}$ from initial to final states $i \to f$ are obtained by integrating the DCS over the solid angle Ω, which at $\hbar \to 0$ is [21]

$$\sigma_{i\to f} = \int_0^{4\pi} \left[\frac{d\sigma(\Omega)}{d\Omega}\right]_{i\to f} d\Omega = 2\pi \int_0^{\infty} P^{i\to f}_{CS}(b) b\, db, \qquad (15)$$

where $P^{i\to f}_{CS}(b) = |S^{i\to f}_{CS}(b)|^2$ is the $i \to f$ transition probability. An important ICS is that for CTR, $H^+ + HC{\equiv}CH \to H^{q=0}$ + other products: σ_{CTR}. As numerically

proven with $H^+ + H_2$ [13], the CTR probability $P_{CS}^{CTR}(b)$ can be accurately obtained from the electron Mulliken population analysis of the outgoing projectile H^q. Mulliken END–CSD/STO-3G σ_{CTR} averaged over the [α, 0°], [α, 45°], [α, 90°] and the whole Set 1 orientations are, 11.0, 11.3, 10.9 and 11.1 Å^2, respectively. A second-order extrapolation to $E_{Lab} = 30$ eV from the three closest available experimental σ_{CTR} [29] is 9.0 Å^2, with lowest experimental error of 1.6 Å^2 [29]. Likewise $H^+ + CH_4$ [14], the present Mulliken σ_{CTR} agrees remarkably well with the experiment.

5. Final remarks

Preliminary results of a complete study of $H^+ + HC{\equiv}CH$ at $E_{Lab} = 30$ eV show that a minimal END–CSD/STO-3G theory employing nuclear frozen Gaussian wave packets at $\hbar \to 0$ and a electronic single-determinantal Thouless CS can satisfactorily describe the system reactivity and predict dynamical properties via CS theory in good agreement with experiments. A complete analysis of these copious simulations will be published soon.

Acknowledgments

Mr. C. Myers was the 2003 Welch Summer Scholar. The authors thank Dr. E. Deumens and Dr. R. Cabrera-Trujillo (University of Florida) for discussions about their END results. Present calculations were done at the Texas Tech University High Performance Computer Center. This work has been partially supported by the Robert A. Welch Foundation grant D-1539 and by an award from the Research Corporation. Also, acknowledgement is made to the donors of The American Chemical Society Petroleum Research fund for partial support of this research.

References

[1] J. Krutein, F. Linder, J. Chem. Phys. 71 (1979) 599.
[2] G. Neidner, M. Noll, J.P. Toennies, C. Schlier, J. Chem. Phys. 87 (1987) 2685.
[3] M. Noll, J.P. Toennies, J. Chem. Phys. 85 (1986) 3313.
[4] B. Friedrich, G. Neidner, M. Noll, J.P. Toennies, J. Chem. Phys. 87 (1987) 5256.
[5] G. Niedner, M. Noll, J.P. Toennies, J. Chem. Phys. 87 (1987) 2067.
[6] N. Aristov, G. Niednerschatteburg, J.P. Toennies, Y.N. Chiu, J. Chem. Phys. 95 (1991) 7969.
[7] Y. Chiu, B. Friedrich, W. Maring, G. Niedner, M. Noll, J.P. Toennies, J. Chem. Phys. 88 (1988) 6814.
[8] U. Gierz, M. Noll, J.P. Toennies, J. Chem. Phys. 83 (1985) 2259.
[9] J.C. Tully, J.K. Preston, J. Chem. Phys. 55 (1971) 562.
[10] M. Baer, G. Niender-Schatterburg, J.P. Toennies, J. Chem. Phys. 91 (1989) 4169.
[11] E. Deumens, A. Diz, R.L. Longo, Y. Öhrn, Rev. Mod. Phys. 66 (1994) 917.
[12] J.A. Morales, A. Diz, E. Deumens, Y. Öhrn, Chem. Phys. Lett. 74 (1995) 392.
[13] J.A. Morales, A. Diz, E. Deumens, Y. Öhrn, J. Chem. Phys. 103 (1995) 9968.
[14] D. Jacquemin, J.A. Morales, E. Deumens, Y. Öhrn, J. Chem. Phys. 107 (1997) 6146.
[15] M. Hedström, J.A. Morales, E. Deumens, Y. Öhrn, Chem. Phys. Lett. 279 (1997) 241.
[16] S.A. Malinovskaya, R. Cabrera-Trujillo, J.R. Sabin, E. Deumens, Y. Ohrn, J. Chem. Phys. 117 (2002) 1103.
[17] J.R. Klauder, B.S. Skagerstam, Coherent States, Applications in Physics and Mathematical Physics, World Scientific, Singapore, 1985.
[18] H. Goldstein, Classical Mechanics, Addison-Wesley, Reading, MA, 1980.
[19] P. Kramer, M. Saraceno, Geometry of The Time-Dependent Variational Principle in Quantum Mechanics, Springler Verlag, New York, 1981.
[20] J.A. Morales, E. Deumens, Y. Öhrn, J. Math. Phys. 40 (1999) 766.
[21] J.A. Morales, Ph.D. thesis, University of Florida, 1997.
[22] D.J. Thouless, Nucl. Phys. 21 (1960) 225.
[23] D.J. Thouless, The Quantum Mechanics of Many-Body Systems, Academic Press, New York and London, 1972.
[24] R. McWeeney, Methods of Molecular Quantum Mechanics, Academic Press, London, 1992.
[25] A. Szabo, N.S. Ostlund, Modern Quantum Chemistry, Dover Publications, Inc., Mineola, NY, 1989.
[26] E. Deumens, Y. Öhrn, B. Wiener, J. Math. Phys. 32 (1991) 1166.
[27] M.S. Child, Molecular Collision Theory, Dover Publications, Inc., Mineola, NY, 1984.
[28] J.N.L. Connor, D. Farrelly, J. Chem. Phys. 75 (1981) 2831.
[29] T. Kusakabe, K. Asahina, A. Iida, Y. Tanaka, Y. Li, G. Hirsch, R.J. Buenker, M. Kimura, H. Tawara, Y. Nakai, Phys. Rev. A 62 (2000) 062715.